Supplementary Information for

Fluid Mediated Communication Among Flexible Micro-posts in Chemically Reactive Solutions

Moslem Moradi [a] *, Oleg E. Shklyaev* [a]*, Wenzheng Shi* [b]*, and Anna C. Balazs* [a,*]

[a] Department of Chemical Engineering, University of Pittsburgh, Pittsburgh, PA, 15261

[b] Courant Institute, New York University, New York, NY, 10012

I. Methods

A. Model of the elastic post

The elastic rod is modeled as a one-dimensional network of nodes connected by elastic bonds. The elastic energy of the connecting bonds is based on the Kirchhoff's rod model and can be written as[1]:

$$E = \frac{1}{2}\int\Big[b_1\Big(\mathbf{D_1}\cdot\frac{\mathrm{d}\mathbf{r}}{\mathrm{d}s}\Big)^2 + b_2\Big(\mathbf{D_2}\cdot\frac{\mathrm{d}\mathbf{r}}{\mathrm{d}s}\Big)^2 + b_3\Big(\mathbf{D_3}\cdot\frac{\mathrm{d}\mathbf{r}}{\mathrm{d}s}-1\Big)^2\Big]\mathrm{d}s$$

$$+\frac{1}{2}\int\Big[a_1\Big(\frac{\mathrm{d}\mathbf{D_2}}{\mathrm{d}s}\cdot\mathbf{D_3}\Big)^2 + a_2\Big(\frac{\mathrm{d}\mathbf{D_3}}{\mathrm{d}s}\cdot\mathbf{D_1}\Big)^2 + a_3\Big(\frac{\mathrm{d}\mathbf{D_1}}{\mathrm{d}s}\cdot\mathbf{D_2}\Big)^2\Big]\mathrm{d}s\,. \qquad \text{(S1)}$$

Here $a_1 = a_2 = \kappa_b$ is the bending modulus and a_3 is the twist modulus of an isotropic rod. Also, $b_1 = b_2$ is the shear force constant and $b_3 = \kappa_s$ is stretching modulus of the rod. $\mathbf{D_1}$, $\mathbf{D_2}$ and $\mathbf{D_3}$ are are the unit orthonormal directors at each node of the post ans s is the arc length along the elastic bonds. The respective dimensions of κ_s and κ_b are force and force$\times L^2$, where L is the length of the rod. The stretching and bending modulus of the rod allows us to parametrize the elastic forces experienced by the nodes of the post.

The steric repulsion forces on the post, $\mathbf{F}_s$ are the sum of the "node-node" (nn) repulsion between two nodes and the repulsion nodes of the any of the six confining walls. The repulsion force between node i and j is given as $\mathbf{F}^{nn}(\mathbf{r}_i - \mathbf{r}_j) = -\nabla U(r)$, where $U(r)$ is the Morse potential:

$$U(r) = \begin{cases} \varepsilon\left(1 - \exp[-\omega(r - r_0)]\right)^2, & r < r_0 \\ 0, & r \geq r_0. \end{cases} \tag{S2}$$

Here, $r = \left|\mathbf{r}_i - \mathbf{r}_j\right|$ is the distance between the position of the i-th node and the repelling object $\mathbf{r}_j$ (other nodes or wall). Also, ε is the strength of the potential, ω is it's width, and r_0 is the equilibrium (and cutoff) distance. The value of r_0 is taken as $1.3\Delta x$, where the lattice Boltzmann unit Δx corresponds to 100μm. The computations are run for over 8×10^6 iterations, corresponding to 3.7 hours of physical time.

B. Estimating flexural rigidity of the posts

Because we explicitly account for the bending and stretching energies of the chain, we can assign flexural rigidity for each post. To estimate the flexural rigidity, we use the one-dimensional linear beam equation[2]. For a cantilever of length L, which is clamped at one end, and a load F that is applied to the free end (see Fig. S1(a)), the analytical solution for the transverse displacement of

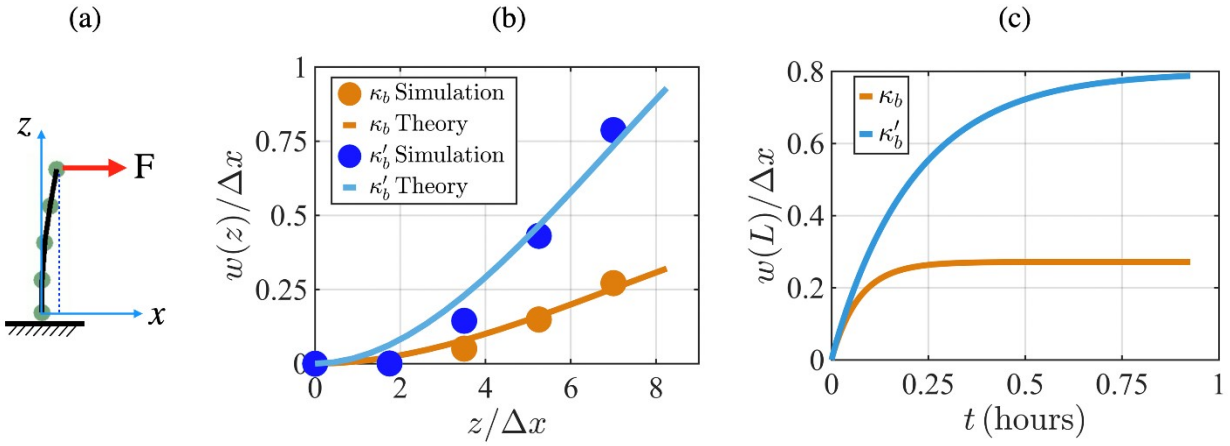

Figure S1 | Estimating bending modulus of the elastic post. (a) Schematic of the post deflection as a result of a constant force. (b) Deflection of the five nodes of the post as a function of vertical position of the nodes from simulation and with the analytical expression for two bending stiffness of the post. (c) Deflection of the top node as a function of time for two bending stiffness of the post. The applied force at the end of the post is $\mathrm{F} = 10^{-14}$ N.

the cantilever is (E is the Young's modulus and I is the second moment of area of the cross section of the post, so that $\mathrm{B} := EI$ is the flexural rigidity of the post):

$$w(x) = \frac{\mathrm{F}}{6EI}(3Lx^2 - x^3). \tag{S3}$$

We compare this analytical solution with the corresponding numerical solution for the transverse displacement of the elastic post. Figure S1(b) shows the final displacements of the nodes from both simulation and theory for posts with two different bending stiffness and Fig. S1(c) shows the deflection of the top node as a function of time for the same two posts. We use the vertical displacement of the end of the post for a given load to compute the flexural rigidity $\mathrm{B} = \dfrac{\mathrm{F}L^3}{3w(L)}$ of the post. We find $\mathrm{B} = 0.04234\, p\mathrm{Nmm}^2$ and $\mathrm{B}' = 0.01429\, p\mathrm{Nmm}^2$, for the two posts, corresponding to bending stiffness of $\kappa_b = 0.17\, p\mathrm{Nmm}^2$ and $\kappa_b' = 0.057\, p\mathrm{Nmm}^2$, respectively. The values of B can be realized experimentally for soft elastic matter on the same size scale[3-5].

II. Supplementary tables

A. Parameters characterizing the chemical reagents

Table S1 Physical properties of chemicals

Chemicals	Density r (g/cc)	Diffusivity D (m^2/s)	Molar mass m_m (g/mol)	Expansion coefficient b (M^{-1})
H_2O	1.00	-	18.015	-
H_2O_2	1.45	1.43×10^{-9}	34.015	0.01056
NaH_2PO_4	2.04	0.88×10^{-9}	119.98	0.07092
$(NH_2)_2CO$	1.32	1.38×10^{-9}	60.06	0.01456
$(NH_4)HCO_3$	1.59	1.48×10^{-9}	79.05	0.02933

Table S2 Parameters for enzymes

Enzyme	k_e (s^{-1})	K_M (M)	$[E]$ (M)
catalase (CAT)	2.1×10^{5}	0.093	0.5×10^{-6}
urease (UR)	23000	0.0013	2.6×10^{-6}

The values for densities and diffusivities are taken from references [6-8]. The values for the enzyme parameters are taken from references[9-12].

B. Parameters characterizing the frequency of passive post oscillation

Post position (Δx)	frequency
$P_1 = (33.5, 27.5)$	$f = 0.82m\text{Hz}$
$P_2 = (34.5, 28.5)$	$f = 1.5m\text{Hz}$
$P_3 = (35.5, 29.5)$	$f = 1.2m\text{Hz}$
$P_4 = (36.5, 30.5)$	$f = 0.98m\text{Hz}$
$P_5 = (37.5, 31.5)$	$f = 0.6m\text{Hz}$

Table S3. Frequency of oscillation of a post at different locations parallel to the diagonal line when the bending stiffness, initial concentration and length of the post are fixed to $\kappa_b = 0.057\,p\text{Nmm}^2$, $C_0 = 50\,m\text{M}$, and $L = 0.8\text{mm}$, respectively.

Concentration	frequency
$C_1 = 1.5C_0 = 75m\text{M}$	$f = 1.3\ m\text{Hz}$
$C_2 = C_0 = 50m\text{M}$	$f = 1.2\ m\text{Hz}$
$C_3 = 0.5C_0 = 25m\text{M}$	$f = 1.05\ m\text{Hz}$

Table S4. Frequency of oscillation of a post in the oscillating point $P = (36.5\Delta x, 28.5\Delta x)$ for different initial concentrations when the length and bending stiffness are fixed to $\kappa_b = 0.057\,p\text{Nmm}^2$ and $L = 0.8\text{mm}$, respectively.

Bending stiffness	frequency
$\kappa_b = 0.057\,p\text{Nmm}^2$	$f = 1.2\ m\text{Hz}$
$\kappa_b = 0.035\,p\text{Nmm}^2$	$f = 0.8\ m\text{Hz}$

Table S5. Frequency of oscillation of a post in the oscillating point $P = (36.5\Delta x, 28.5\Delta x)$ for different bending stiffness when the length and initial concentration are fixed to $L = 0.8\text{mm}$ and $C_0 = 50\,m\text{M}$, respectively.

Post length	frequency
$L = 0.8\text{mm}$	$f = 1.2\ m\text{Hz}$
$L = 0.875\text{mm}$	$f = 1.5\ m\text{Hz}$

Table S6. Frequency of oscillation of a post in the oscillating point $P = (36.5\Delta x, 28.5\Delta x)$ for different post length when the bending stiffness and initial concentration are fixed to $\kappa_b = 0.057\, p\text{Nmm}^2$ and $C_0 = 50\, m\text{M}$, respectively.

Box lateral size (Δx)	frequency
$L_x = L_y = 30$	$f = 1.87\ m\text{Hz}$
$L_x = L_y = 40$	$f = 1.2\ m\text{Hz}$
$L_x = L_y = 60$	$f = 0.6\ m\text{Hz}$
$L_x = L_y = 80$	$f = 0.52\ m\text{Hz}$

Table S7. Frequency of oscillation of a post in oscillating point $P = (36.5\Delta x, 28.5\Delta x)$ for different box lateral sizes when the bending stiffness, initial concentration and length of the post are fixed to $\kappa_b = 0.057\, p\text{Nmm}^2$, $C_0 = 50\, m\text{M}$, and $L = 0.8\text{mm}$, respectively.

III. Supplementary figures

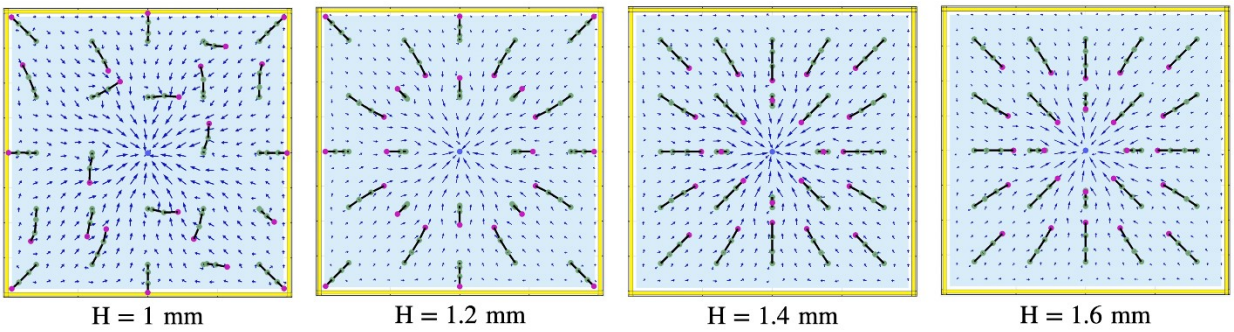

Figure S2 | Top view of the arrangement of an square array of 5×5 elastic posts with one CAT-coated post in the middle for different heights of the chamber: $H = 1\,\text{mm}$, $H = 1.2\,\text{mm}$, $H = 1.4\,\text{mm}$ and $H = 1.6\,\text{mm}$. The length of the post is $L = 0.8\,\text{mm}$ and their bending stiffness is $\kappa_b = 0.057\ p\text{Nmm}^2$. The posts start to oscillate at height $H = 1\,\text{mm}$, and have a steady final configuration for the rest of the heights.

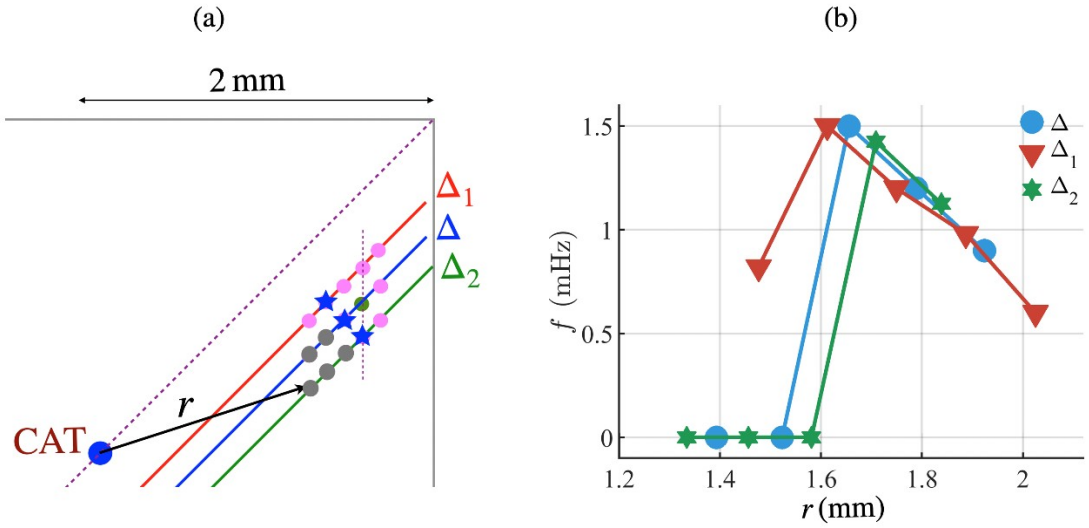

Figure S3 | (a) Schematic top view of the position of passive posts along the lines Δ, Δ_1 and Δ_2 in the first quadrant of chamber with dimensions $4 \times 4 \times 1\,\text{mm}^3$ with one CAT-coated post at the center at different distances from the CAT-coated post. At "star" positions we see maximum frequency of oscillation along each line and at the five gray filled-circles the posts don't oscillate. (b) Frequency of the post oscillation as a function of distance from the CAT-coated post located at different parallel lines Δ, Δ_1 and Δ_2.

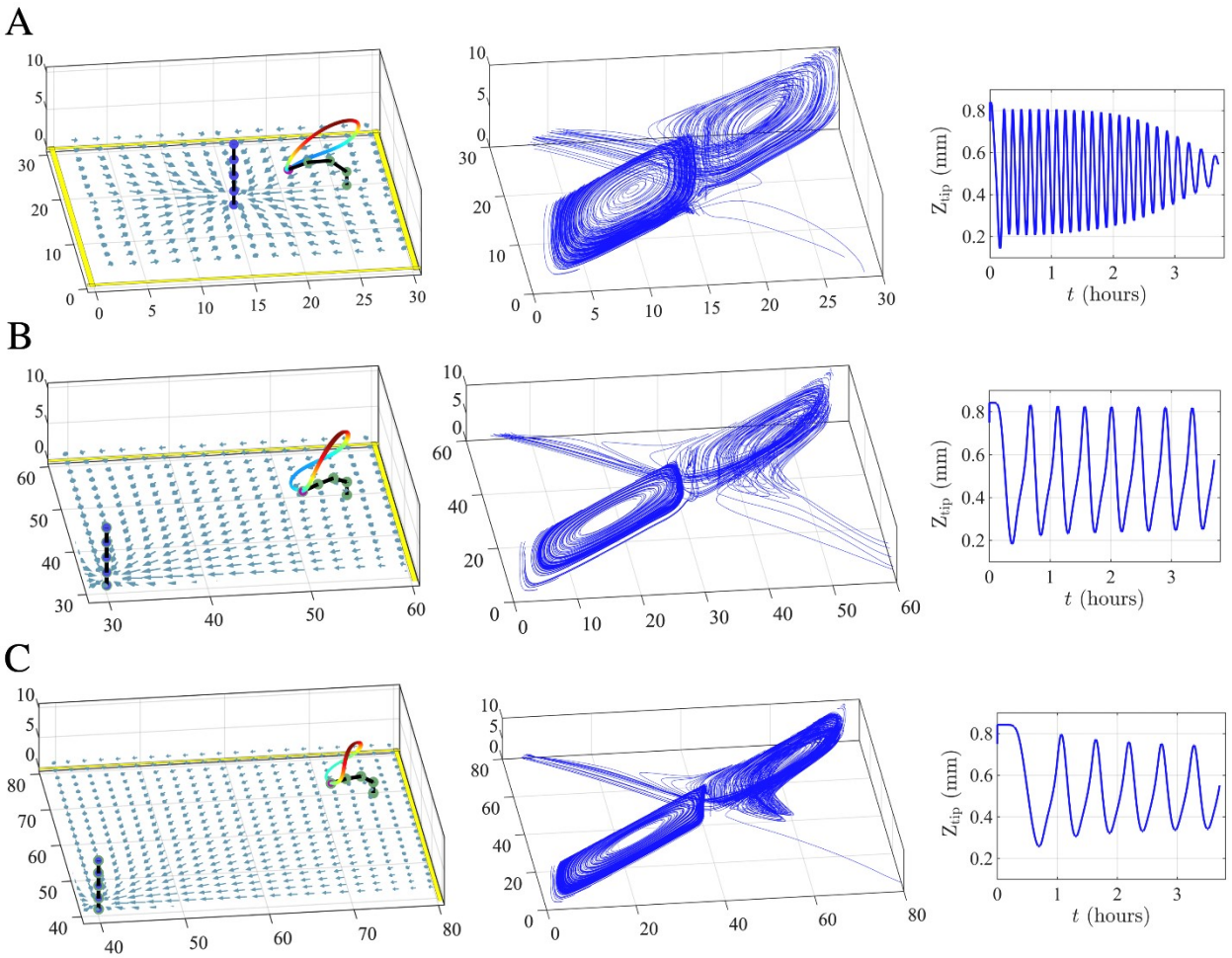

Figure S4 | Oscillation of one passive post due to the flow field generated by one CAT-coated post at the center for different lateral lengths of the chamber: (A) $L_x = L_y = 3\text{mm}$, (B) $L_x = L_y = 6\text{mm}$ and (C) $L_x = L_y = 8\text{mm}$. In the right of each panel, we plot the streamlines along the diagonal plane, and the tip height of the oscillating post as a function of time, respectively. As we increase the lateral box size, the frequency of oscillation decreases. For $L_x = L_y = 3\text{mm}$, we obtain $f = 1.87\,\text{mHz}$; for $L_x = L_y = 6\text{mm}$, we obtain $f = 0.6\,\text{mHz}$, and for $L_x = L_y = 8\text{mm}$, we get $f = 0.52\,\text{mHz}$.

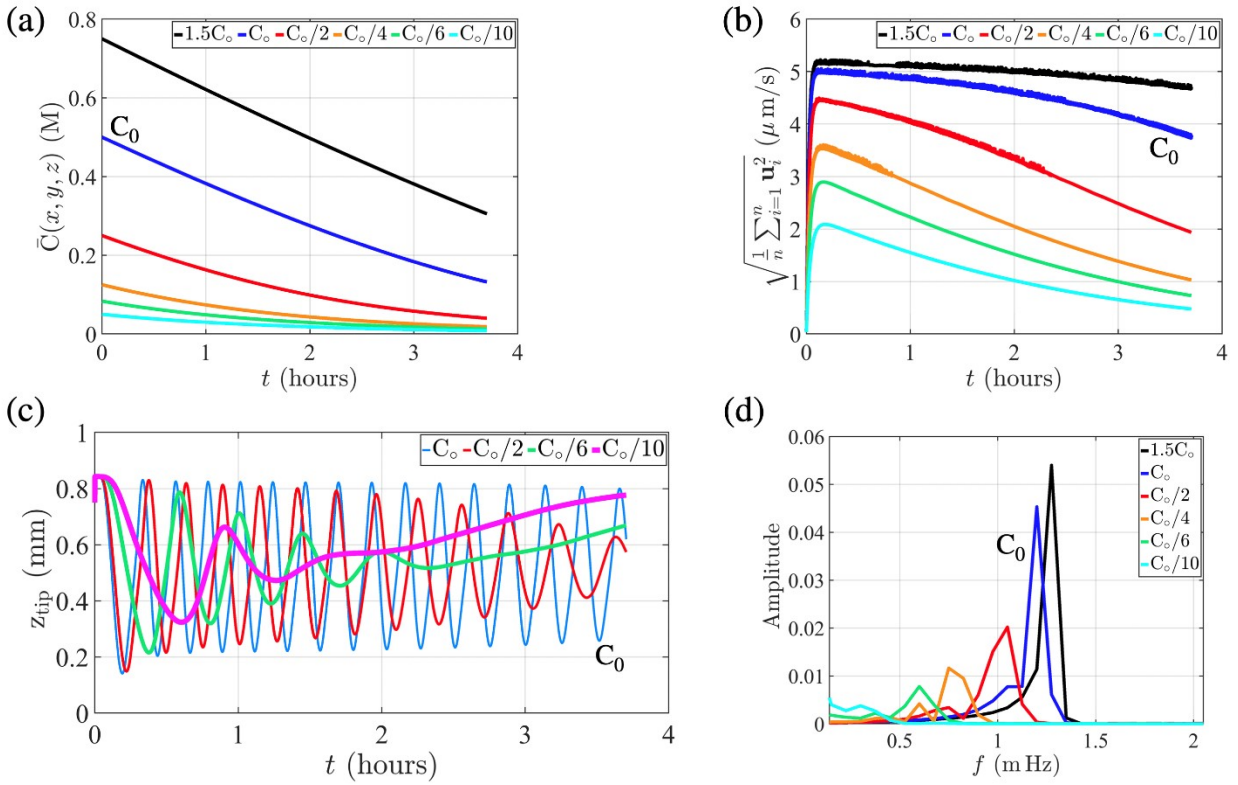

Figure S5 | Effect of changing the initial chemical concentration on the averaged chemical concentration (a), and averaged absolute velocity field (b) in the domain as a function of time, for the case with one CAT-coated post at the center and one passive post near the corner (see Fig. 1, in the main text). (c) Tip height of the oscillating posts as a function of time for different initial chemical concentrations. (d) Frequency of the oscillating post for different initial chemical concentrations. Here, $C_0 = 50\text{mM}$.

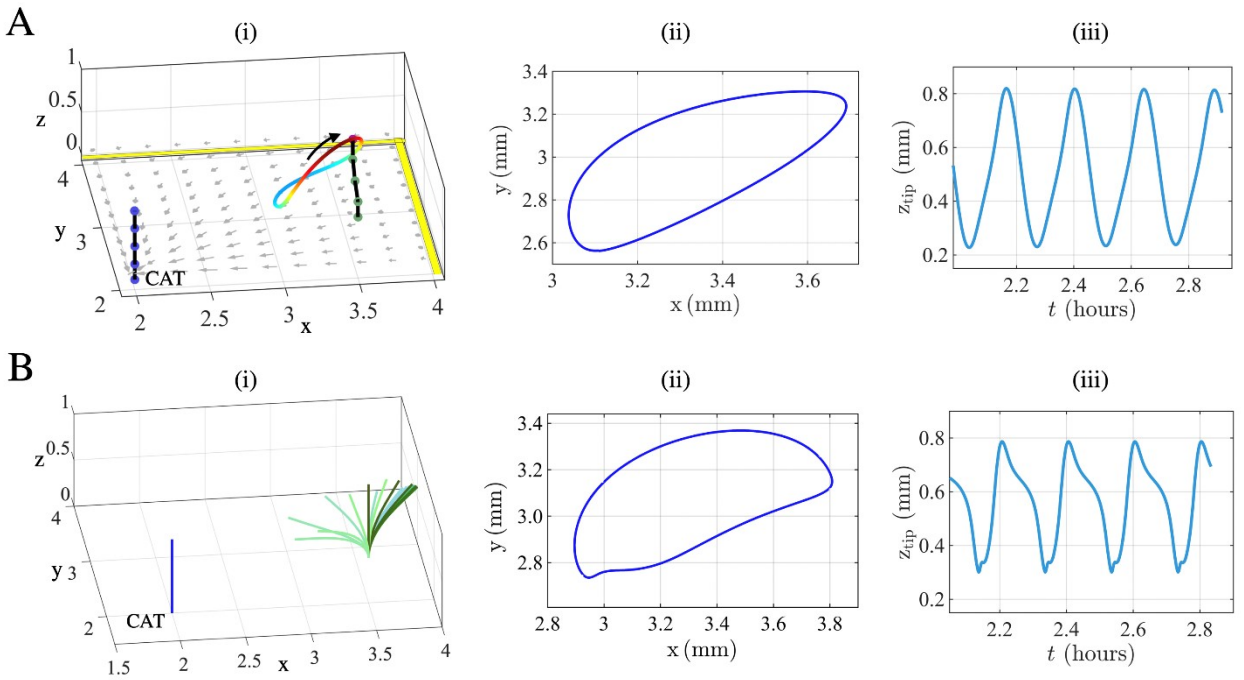

Figure S6 | Oscillation of one passive post due to the flow field generated by one CAT-coated post at the center as obtained by (A) computer simulation and (B) elastohydrodynamic theory. For each panel, on the right, we plot (ii) trajectory of the tip of the passive post projected in x-y plane, and (iii) tip height of the oscillating post as a function of time.

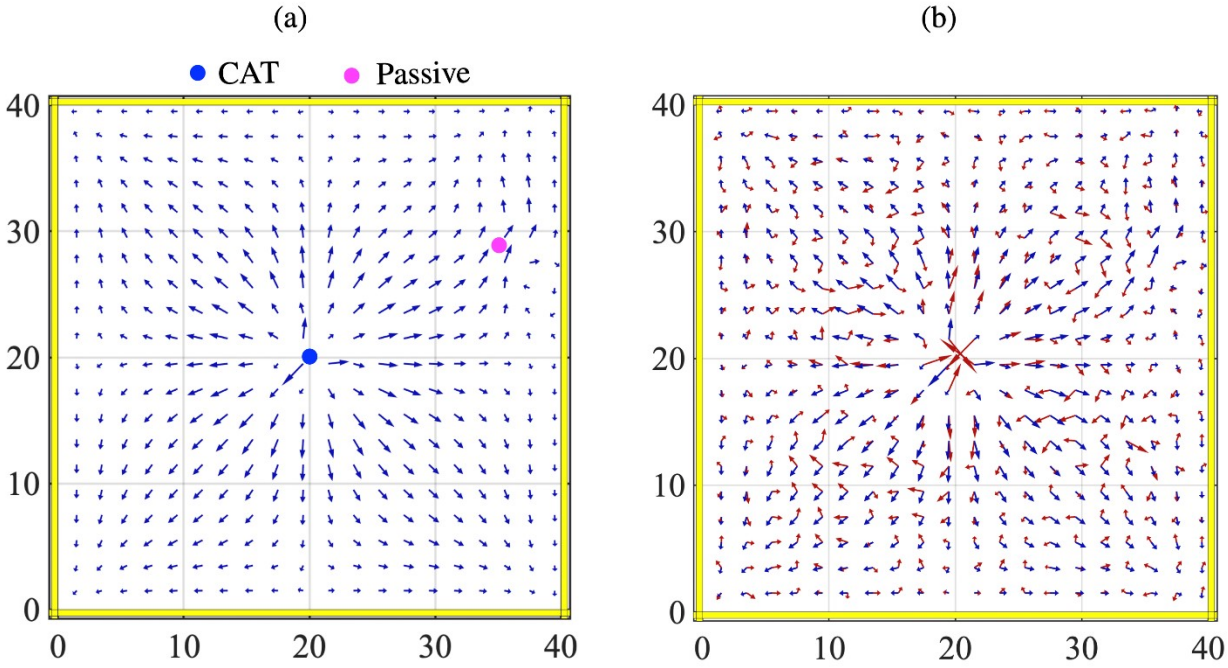

Figure S7 | (a) Top view of the flow field (at $z = 8\Delta x$ plane) generated by one CAT-coated post in the middle of a chamber (colored in blue) in the presence of another passive post at the corner (colored in pink). (b) Top view of the flow field (at $z = 8\Delta x$ plane and colored in red) generated by one CAT-coated post in the middle of a chamber in the presence of 24 passive posts which are located in a 5×5 square array with CAT-coated post at the center. The (a) flow field is plotted (in blue) for comparison.

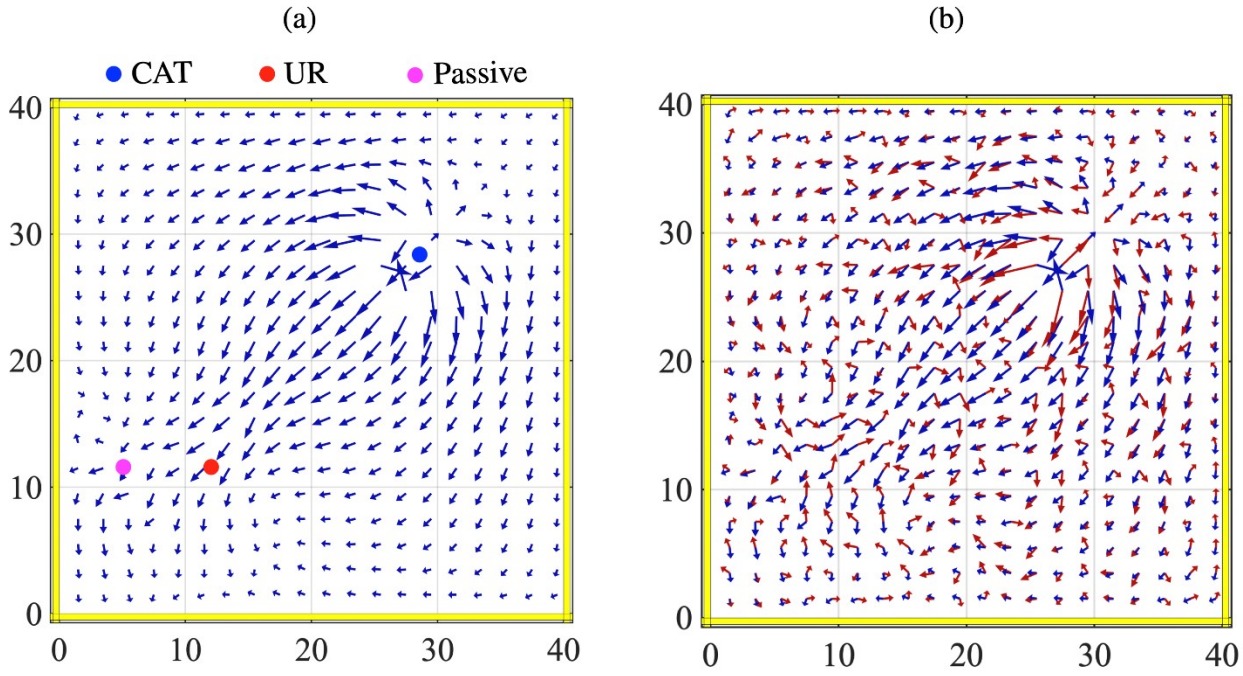

Figure S8 | (a) Top view of the flow field (at $z = 8\Delta x$ plane) generated by one CAT-coated post (colored in blue) and one UR-coated post (colored in red) in the presence of another passive post near UR-coated post (colored in pink). (b) Top view of the flow field (at $z = 8\Delta x$ plane and colored in red) generated by one CAT-coated post and one UR-coated at the same position as in (a), in the presence of 23 passive posts which (together with the two active posts) are located in a 5×5 square array. The (a) flow field is plotted (in blue) for comparison.

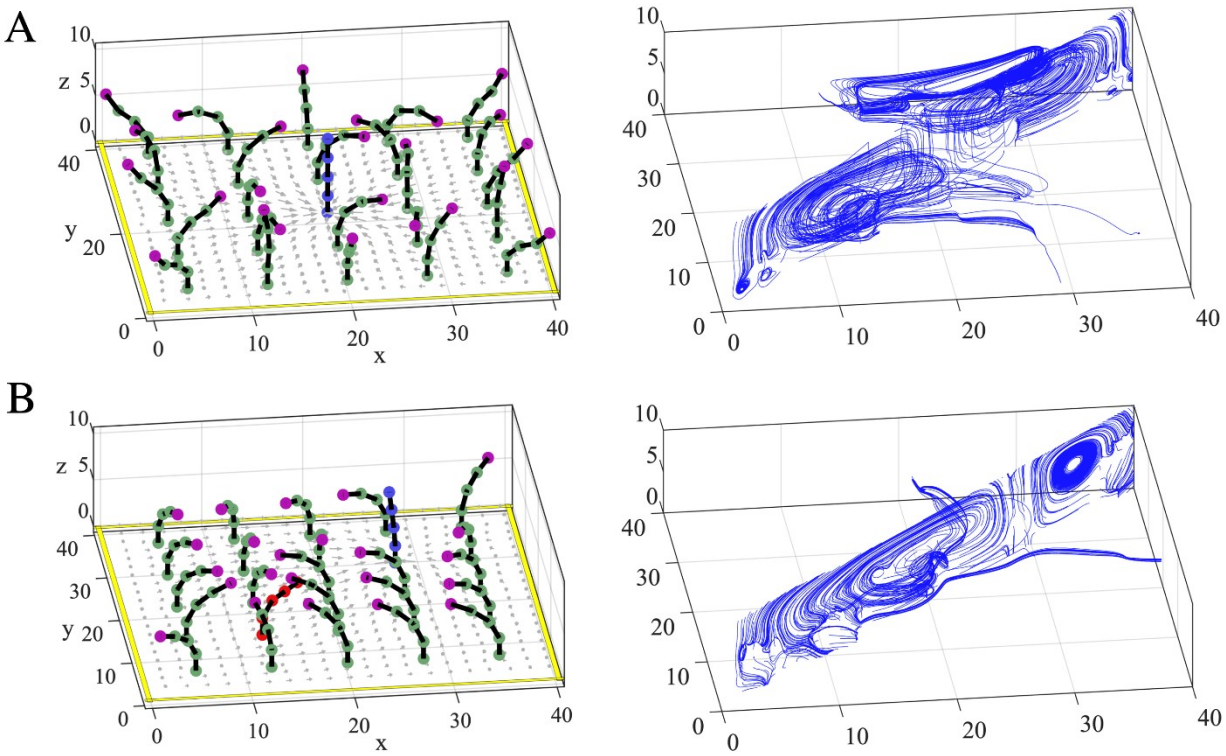

Figure S9 | Top view of the time dependent motion of square array of 5×5 posts with (A) one-CAT-coated post in the middle, and (B) one CAT-coated post and one UR-coated post along the diagonal plane of the chamber. In the right of each panel, we plot the corresponding streamlines in the diagonal plane of the chamber.

IV. Supplementary movies

Supplementary Movie S1: Oscillation of one passive post in presence of one CAT-coated post in the middle of the chamber.

Supplementary Movie S2: Four different modes of motion (stable, unstable, damped and highly damped oscillation) of one passive elastic post at different location of the first quadrant of the chamber.

Supplementary Movie S3: Hydrodynamic communication of two passive elastic posts located at five different oscillating positions in presence of one CAT-coated post at the middle of the chamber.

Supplementary Movie S4: Different modes of motions of UR-coated post for different bending stiffness in a two-active posts system (one CAT-coated post and one UR-coated post), creating a dipolar pattern.

Supplementary Movie S5: Oscillation of posts in a square array of 5×5 posts for two systems: (i) one CAT-coated post at the middle (with 24 passive posts in the square array) and (ii) one CAT-coated post and one UR-coated post along the diagonal plane of the chamber (with 23 passive posts in the square array).

Supplementary Movie S6: Post configurations in an array of 5×5 posts with one CAT-coated post at the middle, for different heights of the chamber (see Fig. S1).

References

1 Lim, S., Ferent, A., Wang, X. S. & Peskin, C. S. Dynamics of a Closed Rod with Twist and Bend in Fluid. *SIAM Journal on Scientific Computing* **31**, 273-302 (2008). https://doi.org:10.1137/070699780

2 Manna, R. K., Shklyaev, O. E. & Balazs, A. C. Chemical pumps and flexible sheets spontaneously form self-regulating oscillators in solution. *Proc Natl Acad Sci U S A* **118** (2021). https://doi.org:10.1073/pnas.2022987118

3 Lin, Y. *et al.* Ultrathin cross-linked nanoparticle membranes. *Journal of the American Chemical Society* **125**, 12690-12691 (2003).

4 Lee, D. Y. *et al.* Macroscopic nanoparticle ribbons and fabrics. *Adv. Mater* **25**, 1248-1253 (2013).

5 Vargo, K. B., Parthasarathy, R. & Hammer, D. A. Self-assembly of tunable protein suprastructures from recombinant oleosin. *Proceedings of the National Academy of Sciences* **109**, 11657-11662 (2012).

6 Haynes, W. M. *CRC handbook of chemistry and physics*. (CRC press, 2014).

7 Luong, T. K. N. *et al.* Multinuclear diffusion NMR spectroscopy and DFT modeling: A powerful combination for unraveling the mechanism of phosphoester bond hydrolysis catalyzed by metal-substituted polyoxometalates. *Chemistry–A European Journal* **21**, 4428-4439 (2015).

8 Larhed, A. W., Artursson, P., Gråsjö, J. & Björk, E. Diffusion of drugs in native and purified gastrointestinal mucus. *Journal of pharmaceutical sciences* **86**, 660-665 (1997).

9 Sengupta, S. *et al.* Self-powered enzyme micropumps. *Nat Chem* **6**, 415-422 (2014). https://doi.org:10.1038/nchem.1895

10 Kruzel, M. & Morawiecka, B. Acid phosphatase of potato tubers (Solanum tuberosum L). Purification, properties, sugar and amino acid composition. *Acta biochimica Polonica* **29**, 321-330 (1982).

11 Ortiz-Rivera, I., Shum, H., Agrawal, A., Sen, A. & Balazs, A. C. Convective flow reversal in self-powered enzyme micropumps. *Proceedings of the National Academy of Sciences* **113**, 2585-2590 (2016).
12 Maiti, S., Shklyaev, O. E., Balazs, A. C. & Sen, A. Self-Organization of Fluids in a Multienzymatic Pump System. *Langmuir* **35**, 3724-3732 (2019). https://doi.org:10.1021/acs.langmuir.8b03607